JACS
JOURNAL OF THE AMERICAN CHEMICAL SOCIETY

Article

pubs.acs.org/JACS

Hydrogen Bond Strength Modulates the Mechanical Strength of Ferric-Thiolate Bonds in Rubredoxin

Peng Zheng,[†] Shin-ichi J. Takayama,[‡] A. Grant Mauk,[‡] and Hongbin Li[†,*]

[†]Department of Chemistry, University of British Columbia, Vancouver, BC V6T 1Z1 Canada

[‡]Department of Biochemistry and Molecular Biology and the Center for Blood Research, University of British Columbia, Vancouver, BC V6T 1Z3 Canada

Supporting Information

ABSTRACT: It has long been recognized that hydrogen bonds formed by protein backbone amides with cysteinyl S^{γ} atoms play important roles in modulating the functional and structural properties of the iron−sulfur centers in proteins. Here we use single molecule atomic force microscopy, cyclic voltammetry, and protein engineering techniques to investigate directly how the strength of N−H···S^{γ} hydrogen bonds in the secondary coordination sphere affects the mechanical stability of Fe(III)-thiolate bonds of rubredoxin. Our results show that the mechanical stability of Fe(III)-thiolate bonds in rubredoxin correlates with the strength of N−H···S^{γ} hydrogen bonds as reflected by the midpoint reduction potential, providing direct evidence that N−H···S^{γ} hydrogen bonds play important roles in modulating the mechanical and kinetic properties of the Fe(III)-thiolate bonds of iron−sulfur proteins and corroborating the important roles of the protein environment in tuning the properties of metal−thiolate bonds.

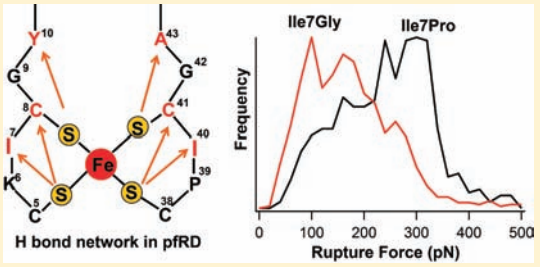

INTRODUCTION

Iron−sulfur proteins are ubiquitous in nature and play critical roles in a wide range of biological processes.[1−4] Facilitated by the highly covalent Fe−S bonds and the unique chemical properties of FeS clusters, iron−sulfur proteins are among the most important electron transfer proteins in nature and exhibit a broad range of reduction potential (−700 to +400 mV). Apart from the intrinsic characteristics of FeS clusters, it has long been recognized that the protein environment modulates the properties of Fe−S bonds to achieve the desired function and stability.[4,5] In particular, protein backbone amides form hydrogen bonds with cysteinyl S^{γ} atoms. These N−H···S^{γ} hydrogen bonds in the secondary coordination sphere are proposed to play important roles in modulating the functional and structural properties of the iron−sulfur centers.[6−8] For example, both crystallography and NMR studies on point mutants of the simplest iron−sulfur protein rubredoxin revealed that the reduction potential of rubredoxin is correlated with the strength of N−H···S^{γ} hydrogen bonds.[9−11] These N−H···S^{γ} hydrogen bonds were also proposed to be responsible for the decreased covalency of Fe(III)-thiolate bonds of rubredoxins relative to their inorganic analogues, as the formation of hydrogen bonds influences electron delocalization between sulfur and iron.[7,12,13] However, direct experimental evidence concerning the quantitative contributions of these backbone hydrogen bonds to the stability of rubredoxins and the strength of Fe(III)-thiolate bonds remains limited.

Over the last two decades, the development of single molecule atomic force microscopy (AFM) has enabled measurement of the mechanical and kinetic properties of chemical bonds (both covalent and noncovalent) at the single molecule level along a well-defined reaction coordinate set by the vector of the applied stretching force.[14−18] Recently, we reported that the stability of a metal−thiolate bond in a protein could be measured for the ferric-thiolate bond at the active site of rubredoxin by single molecule AFM.[19] We found that, despite their highly covalent nature, Fe(III)-thiolate bonds exhibit surprisingly low mechanical stability (~200 pN at a pulling speed of 400 nm/s). Furthermore, the rupture force of ferric-thiolate bonds is much greater than that of Fe(II)-thiolate bonds, and the unfolding force of Fe(III)-thiolate bonds in *Clostridium pasteurianum* rubredoxin (*cp*Rd) is higher than that in *Pyrococcus furiosus* rubredoxin (*pf*Rd). The order of the mechanical stability of Fe−S bonds correlates with bond covalency.

To evaluate the contributions of hydrogen bonds to the properties of Fe−S bonds and the correlation between covalency and mechanical stability in greater depth, we have now combined protein engineering, cyclic voltammetry (CV) and single molecule AFM techniques to test directly whether the strength of hydrogen bonds formed by backbone amides and cysteinyl S^{γ} atoms can modulate the mechanical/kinetic stability of metal−thiolate bonds in the model protein *pf*Rd directly.

MATERIALS AND METHODS

Protein Engineering. The genes encoding the Ile7Pro, Ile7Gly, Ala43Pro and Ala43Gly *pf*-rubredoxin variants were generated by standard site-directed mutagenesis methods using the wild-type

Received: August 19, 2011
Published: February 6, 2012

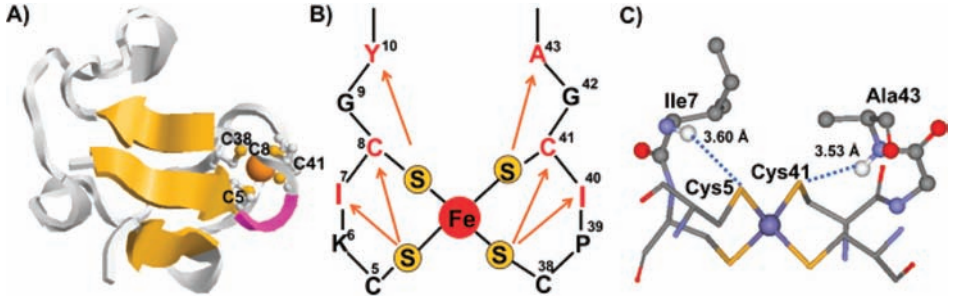

Figure 1. Schematics of the hydrogen bond network formed by backbone amides and cysteinyl S^{γ} atoms in *pf*Rd (PDB:1BRF). (A) Three dimensional structure of *pf*Rd. The three-stranded antiparallel β-sheet structure and the β-turn including Lys6 and Ile7 are highlighted in yellow and pink, respectively. The ferric ion and four cysteine residues are depicted using ball and stick model. Cys5 and Cys38 are interior residues and Cys8 and Cy41 are exterior residues. (B) Cartoon representation of residues in the secondary coordination sphere that are involved in the formation of hydrogen bond with FeS_4 center as identified from X-ray diffraction studies.[29,30] The four cysteinyl S^{γ} atoms are denoted by S, and the other letters are single-letter amino acid designations. (C) Close-up view of the 3D structure of *pf*Rd in the vicinity of the N−H···S^{γ} bond between Ile7 and Cys5 and between Ala43 and Cys41. N−H···S^{γ} bonds are indicated by dashed lines.

pf-rubredoxin gene as the template. Similarly, the genes encoding chimera Cys-Ile7Pro-GB1-Cys, Cys-Ile7Gly-GB1-Cys, Cys-Ala43Pro-GB1-Cys, and Cys-Ala43Gly-GB1-Cys were constructed using Cys-wt-*pf*Rd-GB1-Cys gene as the template. All of these constructs contain an N and C-terminal cysteine residue to facilitate the construction of polyproteins using maleimide−thiol chemistry. The gene was then cloned in the expression vector pQE80L between the *BamHI* and *KpnI* sites, and the construct was confirmed by DNA sequencing. Proteins were overexpressed in *Escherichia coli* strain DH5α and purified by Co^{2+}-affinity chromatography using TALON His-Tag purification resins (Clontech). The protein solution was exchanged into Tris buffer (pH 8.5, 10 mM) using a 9K MWCO Pierce concentrator (Thermo Scientific).

Pure Fe-form rubredoxin variants as well as the rubredoxin-GB1 chimera were purified further by ion-exchange chromatography using a Mono Q 5/50 GL column (GE Healthcare) to remove the coexpressed Zn-form rubredoxin. Polyproteins $(Ile7Pro\text{-}GB1)_n$, $(Ile7Gly\text{-}GB1)_n$, $(Ala43Pro\text{-}GB1)_n$, and $(Ala43Gly\text{-}GB1)_n$ were prepared using a maleimide−thiol coupling reaction by reacting Cys-Ile7Pro-GB1-Cys (or Cys-I7G-GB1-Cys or Cys-Ala43Pro-GB1-Cys or Cys-Ala43Gly-GB1-Cys) with $BM(PEO)_3$ (1, 8-bis (maleimido)triethylene glycol, Molecular Biosciences) specifically as described.[19,20] The degree of polymerization (n) was determined using sodium dodecyl sulfate polyacrylamide gel electrophoresis (SDS-PAGE). The linkages between consecutive Rd-GB1 heterodimers (i.e., head-to-tail, head-to-head and tail-to-tail) in the resulting polyproteins are random. Because the stretching force is a vector, protein domains in the polyprotein will be subject to the same stretching force regardless of their linkages, and thus the AFM measurements are not affected by the orientation of the linkage between consecutive Rd-GB1.[20−22]

Cyclic Voltammetry. CV experiments were carried out with an Autolab PGSTAT12 potentiostat-galvanostat (Eco Chemie, The Netherlands) with an edge-plane pyrolytic carbon working electrode (PGE). The PGE was polished with an alumina slurry and then sonicated in deionized water for 30 s before use. Typically, protein solution (2 μL, 2 mM) was spread onto the surface of the PGE with a microsyringe and then covered with a semipermeable membrane. A saturated calomel (SCE) electrode (Radiometer, France) and platinum wire were used as the reference and counter electrodes, respectively. All experiments were carried out in sodium phosphate buffer (pH 7.0, 200 mM).

UV/vis Absorption Spectroscopy. The electronic absorption spectra of wild-type and variant Rds and of the Rd-GB1 chimeric proteins were recorded in Tris buffer (10 mM, pH 8.5) with a NanoDrop Model ND-1000 spectrophotometer at room temperature. The protein concentration was ~0.5 mM as determined from the absorbance of the solution at 495 nm (ε = 9.22 mM^{-1} cm^{-1}).[23]

Circular Dichroism Spectroscopy. Circular dichroism (CD) spectra were recorded with a Jasco Model J810 spectropolarimeter using a quartz cuvette with a path length of 0.2 cm. For these measurements, protein samples with concentrations of ~1 mM were used. For the far-UV CD measurements, the same protein samples were diluted with distilled water to ~10 μM for measurements.

Single Molecule AFM. Single molecule AFM experiments were performed on a custom-built AFM as reported.[24] The spring constant of each Si_3N_4 cantilever (Bruker Corp.) was calibrated in solution using the equipartition theorem prior to each experiment (typically ~40 pN/nm). All experiments were performed in Tris buffer (pH 7.4) at room temperature.

In a typical experiment, the polyprotein sample (2 μL, 2 mg/mL) was added onto a clean glass coverslip covered by Tris buffer (~50 μL, pH 7.4, 100 mM). The protein was allowed to absorb onto the coverslip for ~5 min before the AFM experiment. The polyprotein was picked up randomly along the contour of the polyprotein by means of nonspecific adhesion with the AFM tip, leading to different number of unfolding force peaks in each force−extension curve. The use of polyproteins and GB1 fingerprint domains in this manner afforded unambiguous identification of single molecule stretching events.[25,26]

Monte Carlo Simulations. The mechanical rupture process of the ferric-thiolate bonds can be modeled as a two-state dissociation process with force-dependent rate constants:[17]

$$\alpha_0 F = \alpha_0 \exp(F\Delta x_u / k_B T)$$

where $\alpha_0 F$ is the rate constant for dissociation at a stretching force F, α_0 is the spontaneous dissociation rate constant at zero force, Δx_u is the distance between the bound and transition states, k_B is the Boltzmann constant, and T is the absolute temperature. We estimated the dissociation rate constant α_0 at zero force and Δx_u by means of Monte Carlo simulations as previously reported.[27,28]

RESULTS

Design of Proline and Glycine Variants of Rubredoxin to Modulate the Strength of N−H···S^{γ} Hydrogen Bonds. In the second coordination sphere of *pf*Rd, multiple residues (Ile7, Cys8, Tyr10, Ile40, Cys41, and Ala43) have been identified to form N−H···S^{γ} hydrogen bonds (Figure 1) that involve backbone amides and the Fe−S center.[29−32] To investigate the effect of hydrogen bond strength on the mechanical properties of Fe(III)-thiolate bonds, we chose residue Ile7 and Ala43 as the sites to introduce point mutations for specific perturbation of the N−H···S^{γ} hydrogen bond strength (Figure 1B,C).

To achieve the greatest possible range of hydrogen bond strength by mutation, proline and glycine substitutions were introduced at both sites (Ile7Pro and Ile7Gly, Ala43Pro and Ala43Gly). Proline is an imino acid and lacks a backbone amide hydrogen to serve as a hydrogen bond donor in the formation of an N−H···S^{γ} hydrogen bond. Introduction of a proline residue has been used previously to assess the role of backbone

dx.doi.org/10.1021/ja2078812 | J. Am. Chem. Soc. 2012, 134, 4124−4131

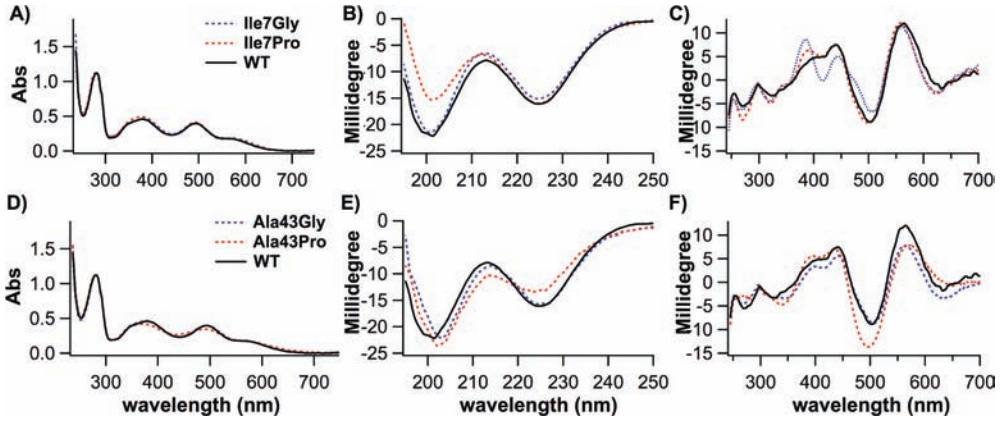

Figure 2. Absorption spectra of rubredoxin variants at positions 7 and 43 compared with wt-*pf*Rd. (A) UV/vis absorption spectra of Ile7Pro and Ile7Gly variants show indistinguishable feature as wt-*pf*Rd. The blue dash line is for Ile7Gly, the red is for Ile7Pro and the black solid line is for wt-*pf*Rd. All three spectra superimpose with each other. (B) Far-UV CD spectra of Ile7Pro and Ile7Gly. (C) UV/vis CD spectrum of Ile7Pro and Ile7Gly. Color coding of the curves is the same for A-C). (D) UV/vis absorption spectra of Ala43Pro and Ala43Gly variants. The blue dash line is for Ala43Gly, the red is for Ala43Pro and the black solid line is for wt-*pf*Rd. All three spectra superimpose with each other. (E) far-UV CD spectra of Ala43Pro and Ala43Gly F) UV/vis CD spectra of Ala43Pro and Ala43Gly. Color coding of the curves is the same for D−F).

hydrogen bonds in protein structure and function, including the blue-copper protein cupredoxin.[33−35] Replacing Ile7 with proline prevents residue 7 from forming an N−H···S^{γ} hydrogen bond with residue Cys5, while replacing Ala43 with proline eliminates the N−H···S^{γ} hydrogen bond between Ala43 and Cys41. However, glycine was shown to form the strongest hydrogen bond N−H···S^{γ} in *cp*Rd, as indicated by NMR and electrochemical analysis.[5,14] Consequently, these two pairs of variants allow assessment of the extremes in strength of the N−H···S^{γ} hydrogen bond that can be formed by residue 7 with Cys5 and by residue 43 with Cys41.

The FeS_4 Centers and the Secondary Structures of All Rubredoxin Variants Remain Largely Intact. To confirm that the FeS_4 center is intact in the engineered rubredoxin variants, we measured the electronic absorption spectra of the ferric form of all four variants (Ile7Pro, Ile7Gly, Ala43Pro, and Ala43Gly). As shown in Figure 2A,D the electronic spectra of the variants are indistinguishable from that of wt-*pf*Rd: all five spectra superimpose with each other and show identical characteristic absorption signals with maxima centered at 390, 495, and 570 nm, which are attributed to the ligand to metal charge-transfer transitions of oxidized rubredoxins.[36] In addition, the A_{495}/A_{280} ratio, which indicates the purity of the Fe-form rubredoxin, is ∼0.36 for all five proteins. These results suggest that neither substitution caused significant structural changes to the FeS_4 center.

Moreover, we also obtained far UV and UV/vis CD spectra to evaluate further the secondary structures of the variants as well as the environments of their aromatic amino acids and Fe(III) site. The far-UV CD spectra of the four variants are similar to that of wt-*pf*Rd, suggesting that the three-stranded antiparallel β-sheet structure remains largely intact (Figure 2A). The change of the band at 200 nm for Ile7Pro is consistent with the anticipated influence of the proline substitution on the β-turn structure. The CD spectra of the four variants in the visible range are also similar to that of wt-*pf*Rd and exhibit highly similar patterns with maxima at 320 nm (−), 350 nm (−), 400 nm (+), 440 nm (+), 505 nm (−), 560 nm (+), and 630 nm (−). This feature is also very similar to that observed for rubredoxins from other species.[37,38] The intensities of several transitions differ notably among the variants (wt-*pf*Rd, Ile7Pro, Ile7Gly, Ala43Pro, and Ala43Gly), an observation that may also result from fine-tuning of the FeS_4 center by mutation-induced alteration of hydrogen bond strength.

Cyclic Voltammetry Confirms the Relative Order of the Hydrogen Bond Strength of the Three *pf*Rd Variants. To confirm the order of hydrogen bond strengths of the pairs of rubredoxin variants at residues 7 and 43 (proline variant versus glycine variant) relative to wt-*pf*Rd, we undertook CV measurements to determine the reduction potentials of all variants as well as the wild-type protein because the reduction potential is correlated with the strength of the N−H···S^{γ} hydrogen bond.[5,14] A weaker H bond to the sulfur atom leads to a lower reduction potential. As shown in Figure 3A, the CVs of Ile7Pro shifted to a significantly lower

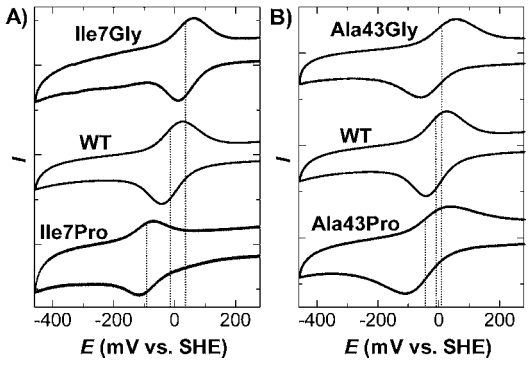

Figure 3. Reduction potential of *pf*Rd variants measured by CV. The protein was entrapped between the surface of a pyrolytic graphic electrode and a semipermeable membrane (sodium phosphate buffer (200 mM, pH 7.0, 20 °C)). Scan rate, 50 mV/s. (A) Compared with wt-*pf*Rd, the Ile7Pro shows a significantly lower reduction potential while Ile7Gly shows a higher reduction potential. This result suggests that the strength of the N−H···S^{γ} hydrogen bond increases following the order Ile7Pro < wt < Ile7Gly. (B) CV measurement on the Ala43Pro and Alal43Gly shows a similar trend in reduction potential shift.

reduction potential than observed for wt-*pf*Rd (−91 mV vs SHE (standard hydrogen electrode) for Ile7Pro vs −4 mV for wt), while the Ile7Gly variant exhibited a much higher reduction potential (42 mV vs SHE). Substitutions at residue

dx.doi.org/10.1021/ja2078812 | *J. Am. Chem. Soc.* 2012, 134, 4124−4131

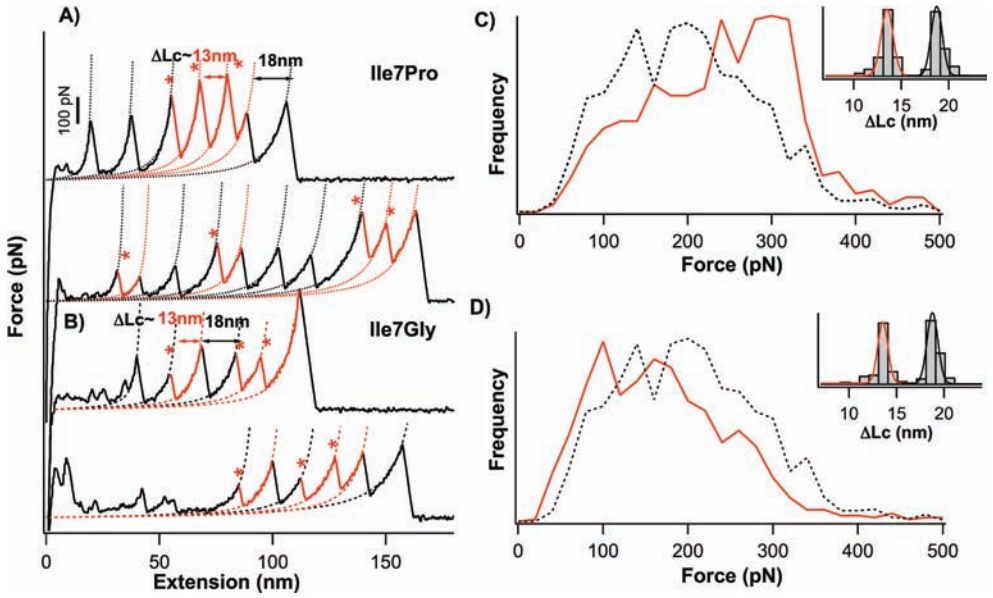

Figure 4. Mechanical unfolding of polyprotein chimera $(Ile7Pro\text{-}GB1)_n$ and $(Ile7Gly\text{-}GB1)_n$ demonstrates that the mechanical strength of Fe(III)-thiolate bonds increases with a decrease in the hydrogen bond strength. (A,B) Typical force−extension curves of $(Ile7Pro\text{-}GB1)_n$ (A) and $(Ile7Gly\text{-}GB1)_n$ (B). The unfolding events of Ile7Pro and Ile7Gly are of ΔL_c of ∼13 nm and colored in red and indicated by *. The unfolding events of the fingerprint GB1 domains are of ΔL_c of ∼18 nm and colored in black. (C,D) Histograms of the mechanical rupture forces of Fe(III)-thiolate bonds in Ile7Pro (C) and Ile7Gly (D). The bin size is 20 pN. The average rupture force of Fe-thiolate bonds is 255 ± 4 pN for Ile7Pro (n = 564, ave. ± standard error of the mean) and 182 ± 3 pN for Ile7Gly (n = 829), respectively. For comparison, the rupture force histogram of Fe(III)-thiolate bonds in wt-*pf*Rd is also shown (black dashed line, average rupture force of 214 pN). The inset is the ΔL_c histogram of the mechanical unfolding of the corresponding polyprotein chimera. The solid lines are Gaussian fits to the experimental data. The peak centered at ∼13 nm corresponds to the unfolding of pfRd variants, while the peak centered at ∼18 nm corresponds to the unfolding of the fingerprint GB1 domains.

43 resulted in similar shifts in reduction potential: Ala43Pro(−40 mV) < wt(−4 mV) < Ala43Gly(13 mV) (Figure 3B). These results provide strong support for the conclusion that the glycine substitution strengthens the N−H···S^{γ} hydrogen bond significantly while the hydrogen bond is significantly weakened by proline substitution. This conclusion is consistent with the anticipated effect of a proline substitution to prevent the formation of an N−H···S^{γ} hydrogen bond.

Single Molecule AFM Experiments Reveal the Effect of the Hydrogen Bond Strength on the Mechanical Stability of the Ferric-Thiolate Bond. Having established the hydrogen bond strengths of these *pf*Rd variants, we used single molecule AFM to measure the mechanical stability of the ferric-thiolate bond in both *pf*Rd variants. To identify single molecule stretching events unambiguously, we employed the well-established fingerprint polyprotein chimera approach and constructed polyprotein chimeras $(Rdmutant\text{-}GB1)_n$, in which the well-characterized GB1 domain serves as a fingerprint for identifying single molecule stretching events as well as an internal force caliper for the rupture force measurements of the ferric-thiolate bonds of rubredoxin.[19,39,40] We obtained electronic absorption and CD spectra (both far UV and UV/vis) of the Rdmutant-GB1 protein chimeras and confirmed that as indicated by these criteria, the presence of GB1 in Rd-GB1 chimera does not perturb the structure or electronic properties of the FeS_4 center relative to those of native rubredoxin (Figures S1−S3 of the Supporting Information, SI).

We then used a maleimide−thiol coupling reaction to construct polyprotein chimeras $(Rdmutant\text{-}GB1)_n$ by reacting each Rdmutant-GB1 chimera which carries a cysteine residue at its N- and C-termini, with $BM(PEO)_3$.[19,20] The degree of polymerization n ranges from 2 to 5, as determined from sodium dodecyl sulfate polyacrylamide gel electrophoresis (SDS-PAGE) (Figure S4 of the SI). This result is similar to previous results for polyproteins constructed using the disulfide approach[21,22] or thiol-maleimide chemistry.[20] Although the dominant forms are dimers and trimers, polyproteins of higher degree of polymerization are clearly observed by SDS-PAGE. Because the heterogeneity of the length of the polyprotein has little effect on the measured unfolding force of proteins,[21,41] the resulting polyproteins were used directly in the AFM pulling experiments without further purification. Moreover, the thiol-maleimide coupling reaction does not affect the properties of the FeS_4 centers of the Rd domains coupled within the polyproteins (Figure S5 of the SI).

As shown in Figure 4A, stretching the polyprotein chimera $((Ile7Pro\text{-}GB1)_n$ resulted in characteristic sawtooth-like force−extension curves in which each force peak corresponds to the unfolding of each domain. Fitting the force−extension curves to the Worm-like Chain model of polymer elasticity[42] revealed that the unfolding force peaks exhibit two distinct types of contour length increment (ΔL_c): 18 and 13 nm (Figure 4A). The mechanical unfolding of the fingerprint GB1 domains, which has been studied in detail,[29,30] is characterized by ΔL_c of ∼18 nm. Thus, unfolding events with ΔL_c of 18 nm can be readily attributed to the unfolding of GB1 domains.[19,39,40] Because Ile7Pro alternates with GB1 domains in the polyprotein chimera, unfolding events of ΔLc of 13 nm can accordingly be assigned to the unfolding of Ile7Pro without any ambiguity. The contour length increment of Ile7Pro (13 nm) is identical to that of wt-*pf*Rd and is consistent with the anticipated length increase resulting from rupture of the FeS_4 center.[19,20] In our previous study,[19,20] we showed that the unfolding of apo-rubredoxin itself does not contribute to the measured unfolding force of holo-Rd as the apo-Rd unfolds at forces <20 pN. Therefore, the major event during the

dx.doi.org/10.1021/ja2078812 | J. Am. Chem. Soc. 2012, 134, 4124−4131

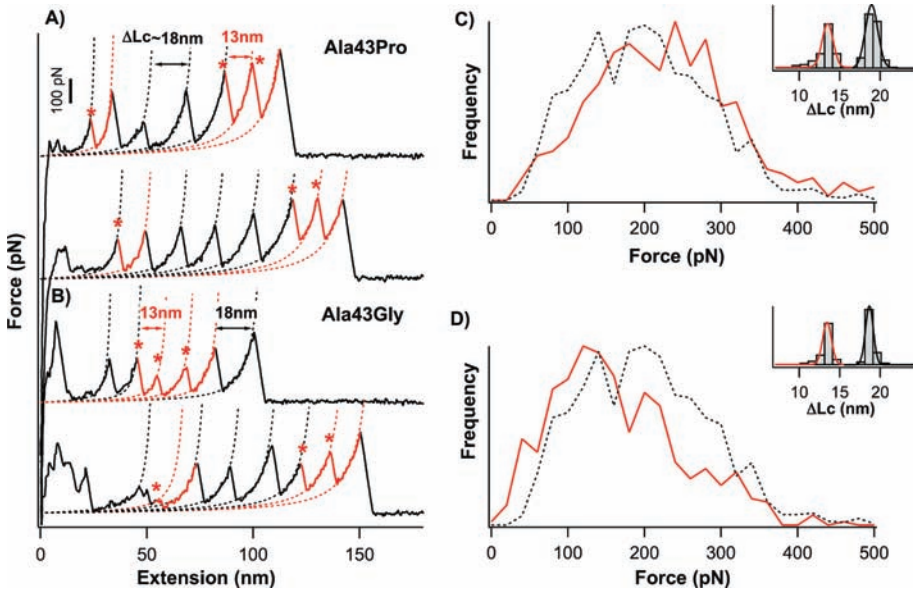

Figure 5. Mechanical unfolding of polyprotein chimeras $(Ala43Pro\text{-}GB1)_n$ and $(Ala43Gly\text{-}GB1)_n$. Typical force−extension curves of (A) $(Ala43Pro\text{-}GB1)_n$ and (B) $(Ala43Gly\text{-}GB1)_n$. The unfolding events of Ala43Pro and Ala43Gly exhibit ΔL_c of ∼13 nm and are shown in red (indicated by *). The unfolding events of the GB1 fingerprint domains exhibit ΔL_c of ∼18 nm and are shown in black. (C,D) Histogram of the mechanical rupture forces of Fe(III)-thiolate bonds in (C) Ile43Pro and(D) Ile43Gly. The bin size is 20 pN. The average rupture force of Fe-thiolate bonds is 248 ± 6 pN for Ala43Pro (n = 425) and 182 ± 4 pN for Ala43Gly (n = 482), respectively. It is clear that a much greater rupture force is required for the Ala43Pro variant than for the Ala43Gly variant. For comparison, the rupture force histogram of the ferric-thiolate bond in wt-*pf*Rd is also shown (black dashed line). The inset is the histogram of the ΔL_c of the mechanical unfolding of the corresponding polyprotein chimera.

mechanical unfolding of the Ile7Pro variant can be readily assigned to the mechanical rupture of the FeS_4 center in this protein domain, and the unfolding force of Ile7Pro variant can be attributed to the rupture force of the FeS_4 center in the Ile7Pro domain.[43] It is of note that at least two mechanisms of rupturing FeS_4 center in rubredoxin (including "pulling apart" of the peptide segments, CXXC chelation loops and N−H···S^{γ} bonds) are possible. However, due to the limited resolution of the AFM, current data are insufficient to select between the two possible mechanisms (Figure S6 of the SI).

As shown in Figure 4C, the rupture force of FeS_4 in Ile7Pro exhibited a broad distribution that reflects the intrinsically short distance between the bound state and rupture transition state.[17,19] However, the average rupture force of the Ile7Pro variant is shifted toward a higher value [255 ± 4 pN for Ile7Pro (n = 564) versus 214 ± 3 pN for wt (n = 1534), the data are represented as mean ± standard error of the mean, where n represents the number of independent observations], suggesting that eliminating the N−H···S^{γ} hydrogen bond increases the mechanical stability of Fe(III)-thiolate bonds.

Similar analysis of the Ile7Gly variant revealed that the Fe(III)-thiolate bond of this variant ruptures at a lower force of 182 ± 3 pN (n = 829), suggesting that increased N−H···S^{γ} bond strength leads to a decrease in the mechanical stability of Fe(III)-thiolate bonds. These results are consistent with the conclusion that the strength of the N−H···S^{γ} hydrogen bond indeed modulates the mechanical strength of the ferric-thiolate bonds of *pf*Rd.

To evaluate the generality of this effect, we undertook similar single molecule AFM analyses of *pf*Rd variants with substitutions for residue 43. Single molecule AFM experiments of the polyprotein chimeras $(Ala43Pro\text{-}GB1)_n$ and $(Ala43Gly\text{-}GB1)_n$ exhibited the expected increase in the mechanical unfolding force for Ala43Pro (248 ± 6 pN, n = 425) as well as the expected decrease for Ala43Gly (182 ± 4 pN, n = 482) (Figure 5). These results for both pairs of variants reveal the correlation between the reduction potential and the mechanical rupture force for ferric-thiolate bonds in *pf*Rd (Figure 6),

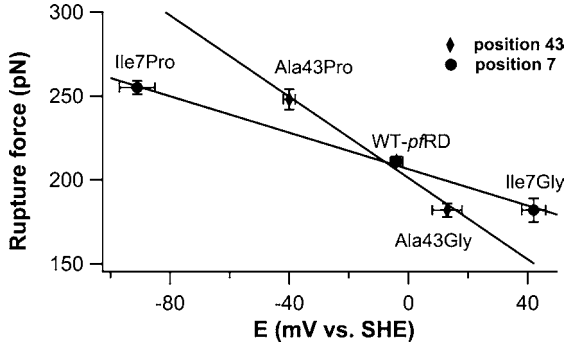

Figure 6. Dependence of the mechanical rupture force of the ferric-thiolate bond in *pf*Rd and its variants on reduction potential: (◆) position 43 variants; (●) position 7 variants. The solid lines are linear fits to the data.

suggesting that this modulating effect is a general feature for rubredoxins.

We also carried out the mechanical rupture experiments at various pulling speeds (Figure 7). The dependence of the rupture force on the pulling speed exhibited by all variants remains, within experimental error, similar to that of wt-*pf*Rd, suggesting that the distance between the bound state and the mechanical rupture transition state Δx_u remains unchanged (0.14 nm) in both variants and that the difference in mechanical stabilities of ferric-thiolate bonds of the *pf*Rd variants studied here is largely attributable to the change of the lifetime of ferric-thiolate bonds at zero force. Monte Carlo simulations revealed that the average spontaneous dissociation

dx.doi.org/10.1021/ja2078812 | *J. Am. Chem. Soc.* 2012, 134, 4124−4131

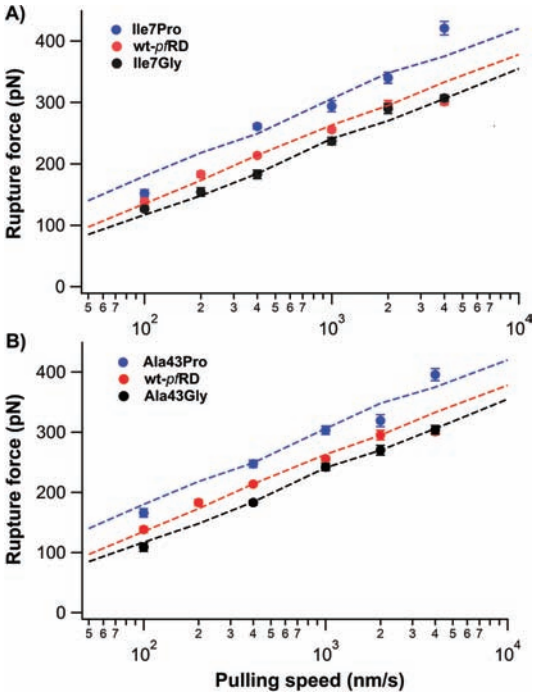

Figure 7. Dependence of the mechanical rupture force of ferric-thiolate bonds in *pf*RD variants on pulling speeds. The rupture forces of the Ile7Pro and Ile7Gly variants exhibited similar speed dependence to that of wt-*pf*Rd, suggesting that the distance between the bound state and mechanical rupture transition state Δx_u remains largely unchanged by the substitutions.

rate constant of the Fe(III)-thiolate bond at zero force is 0.06 s^{-1} for Ile7Pro and Ala43Pro, 0.15 s^{-1} for wt and 0.25 s^{-1} for Ile7Gly and Ala43Gly, respectively.

DISCUSSION

Direct Experimental Evidence Demonstrates that Hydrogen Bond Strength Modulates the Mechanical Stability of Ferric-Thiolate Bonds. Combining protein engineering, cyclic voltammetry, and single molecule AFM techniques, we have demonstrated that the mechanical stability of the ferric-thiolate bond is correlated with the reduction potentials of *pf*Rd variants. Because the reduction potential correlates with the strength of hydrogen bonds, our results provide direct experimental evidence that the strength of the N−H···S^{γ} hydrogen bonds involving the protein backbone amide and cysteinyl S^{γ} atoms can play important roles in modulating the mechanical and kinetic properties of the ferric-thiolate bonds of iron−sulfur proteins. These results demonstrate another important role that the protein environment plays in tuning the properties of metal−thiolate bonds.[44] To the best of our knowledge, the correlation of hydrogen bond strength with mechanical properties of ferric-thiolate bonds in metalloproteins has not been reported previously. It is now clear that the electron delocalization between sulfur and Fe atoms, which can be modulated by N−H···S^{γ} hydrogen bonds, directly determines the mechanical stability of Fe(III)-thiolate bonds (also see note[45]). This conclusion is consistent with our observation that mechanical stability of Fe(III)-thiolate bonds is correlated with bond covalency.[19]

It is well-known that hydrogen bonds from the secondary coordination sphere that are widely observed in many different metalloproteins, play important roles in regulating the biological functions of metalloproteins.[2,6,13] Our current results demonstrate the utility of single molecule AFM in investigating the effect of such hydrogen bonds on active site stabilities of rubredoxin. We anticipate that this method can be applied to other metalloproteins to quantify the roles of these hydrogen bonds in modulating the stability of metal centers.

Furthermore, our experiments also provide potentially interesting model systems for spectroscopic studies of metal−thiolate bonds. It has long been proposed that the relatively low covalency of Fe(III)-thiolate bonds in rubredoxin is attributable to hydrogen bonding interactions formed with the sulfur atoms,[12,46] The variants we report here exhibit a broad range of reduction potential, mechanical stability, and N−H···S^{γ} hydrogen bond strength that should serve as useful models for further use in K-edge X-ray absorption spectroscopy experiments to test this hypothesis in greater depth.

The Influence of Backbone Hydrogen Bonds on the Mechanical Stability of Ferric-thiolate Bond is Site Dependent. Although mutations at two different positions, Ile7 and Ala43, affect the mechanical stability of the ferric-thiolate bond in rubredoxin, we note that the modulation of mechanical strength is more sensitive to the change of reduction potential at residue 43 than that at residue 7 (Figure 6). The experimental slopes observed for this dependence were 1.24 pN/mV for the Ala43 series and 0.55 pN/mV for the Ile7 series. This observation suggests a site-dependent relationship between the hydrogen bond strength and mechanical stability of ferric-thiolate bond in rubredoxin. It is interesting to note that NMR studies of *cp*Rd also revealed a similar site-dependent relationship between hydrogen bond strength and reduction potential for variants at residue 44 (equivalent to the residue 43 series in *pf*Rd (*cp*Rd possesses an additional Met residue at the N-terminus)) and variants at residue 8 (equivalent to residue 7 in *pf*Rd).[11]

Residues Ile7 and Ala43 in *pf*Rd (or residues 8 and 44 in *cp*Rd) exhibit considerably different structural characteristics.[9,11,47] Ile7 is located within the bicysteine coordination loop C5XXC8, which forms a rigid turn structure around the iron atom. In contrast, Ala43 is outside the C38XXC41 coordination loop and is subject to lesser steric strain upon mutation. Thus, it is possible that the site-specific effects on the mechanical stability of ferric-thiolate bond observed here arise from these structural differences.

Another possible basis for the functional inequivalence of these two sites is distinct difference in location of the two cysteine residues that are hydrogen bonded to residues 7 and 43 (Figure 1) in that Cys5 is located at an interior position and Cys41 has a more exterior location. These two cysteines may play different roles during the mechanical rupture of FeS_4 center upon rubredoxin unfolding. Our previous results for variants of *pf*Rd in which Cys residues were replaced with His showed that the shorter Fe-thiolate bonds (Fe-Cys8 and Fe-Cys41) exhibit greater mechanical stability than do the longer Fe-thiolate bonds (Fe-Cys5 and Fe-Cys38).[19] In addition, the hydrogen bond distance between Ile7 and Cys5 (3.60 Å) is greater than the hydrogen bond distance between Ala43 and Cys41 (3.53 Å). Thus, it is likely that the mechanical stability of the FeS_4 center is more sensitive to changes at residue 43, as residue 43 is hydrogen bonded to Cys41.

It is important to note that the effect of active site substitutions on the N−H···S^{γ} hydrogen bond strength is complex. Detailed NMR studies of *cp*Rd showed that substitutions of this type can have localized or aggregate effect on hydrogen bond strength.[11] For example, replacements for Val8 in *cp*Rd resulted in an

dx.doi.org/10.1021/ja2078812 | J. Am. Chem. Soc. 2012, 134, 4124−4131

aggregate effect on the strength of multiple hydrogen bonds that are not only localized to Cys6. In contrast, the effect of substitutions for Val44 can be largely attributed to Cys42 alone. Thus, it is also plausible that multiple factors are responsible for the observed site-dependent relationship between the hydrogen bond strength and mechanical stability of ferric-thiolate bond.

CONCLUSIONS

Using single molecule atomic force microscopy, cyclic voltammetry and protein engineering techniques, we have directly investigated how the strength of N−H···S$^{\gamma}$ hydrogen bonds in the secondary coordination sphere affects the mechanical stability of Fe(III)-thiolate bonds of rubredoxin by substitution of proline or glycine residues for two residues that form hydrogen bonds with the iron atom. Our results demonstrate that the mechanical stability of Fe(III)-thiolate bonds in rubredoxin correlates with the strength of N−H···S$^{\gamma}$ hydrogen bonds, as reflected by the midpoint reduction potential, and thus provide direct experimental evidence that N−H···S$^{\gamma}$ hydrogen bonds play important roles in modulating the mechanical and kinetic properties of the Fe(III)-thiolate bonds of iron−sulfur proteins. These results provide new insight into the influence that the protein environment plays in controlling the properties of metal−thiolate bonds. Furthermore, our work demonstrates the utility of the single molecule AFM in investigating the effect of such hydrogen bonds on active site stabilities of rubredoxin, and we anticipate that this method can be applied to other metalloproteins to quantify the roles of these hydrogen bonds and the protein environment in general in modulating the stability of metal centers in proteins.

ASSOCIATED CONTENT

Supporting Information

The UV−vis absorption spectra of all four Rdmutant-GB1 chimeras; the far-UV CD spectra of the standalone wt-Rd, GB1 and their chimera protein Rd-GB1; the temperature-dependent far-UV and Visible CD spectra of the chimera protein Rd-GB1; SDS-PAGE of the polyproteins $(\text{Rdmutant-GB1})_n$; UV−vis absorption spectrum of $(\text{Rd-GB1})_n$ suggests that the maleimide−thiol coupling reaction does not affect the properties of the FeS_4 center in rubredoxin; two possible mechanisms of rupturing FeS_4 center in rubredoxin. This material is available free of charge via the Internet at http://pubs.acs.org.

AUTHOR INFORMATION

Corresponding Author

Hongbin@chem.ubc.ca

Notes

The authors declare no competing financial interest.

ACKNOWLEDGMENTS

This work was supported by the Natural Sciences and Engineering Research Council of Canada (H.L.), Canada Foundation for Innovation, and Canada Research Chairs (H.L. and A.G.M.).

ABBREVIATIONS

*cp*Rd, *Clostridium pasteurianum* Rubredoxin; *pf*Rd, *Pyrococcus furiosus* Rubredoxin; AFM, atomic force microscopy; CV, cyclic voltammetry; SHE, standard hydrogen electrode

REFERENCES

(1) Beinert, H. *J. Biol. Inorg. Chem.* **2000**, *5*, 2.
(2) Lippard, S. J.; Berg, J. M. *Principles of Bioinorganic Chemistry*; University Science Books: Sausalito, CA, 1994.
(3) Holm, R. H.; Kennepohl, P.; Solomon, E. I. *Chem. Rev.* **1996**, *96*, 2239.
(4) Johnson, D. C.; Dean, D. R.; Smith, A. D.; Johnson, M. K. *Annu. Rev. Biochem.* **2005**, *74*, 247.
(5) Kennepohl, P.; Solomon, E. I. *Inorg. Chem.* **2003**, *42*, 689.
(6) Dey, A.; Okamura, T.-a.; Ueyama, N.; Hedman, B.; Hodgson, K. O.; Solomon, E. I. *J. Am. Chem. Soc.* **2005**, *127*, 12046.
(7) Gamiz-Hernandez, A. P.; Galstyan, A. S.; Knapp, E.-W. *J. Chem. Theory Comput.* **2009**, *5*, 2898.
(8) Lu, Y.; Yeung, N.; Sieracki, N.; Marshall, N. M. *Nature* **2009**, *460*, 855.
(9) Eidsness, M. K.; Burden, A. E.; Richie, K. A.; Kurtz, D. M. Jr.; Scott, R. A.; Smith, E. T.; Ichiye, T.; Beard, B.; Min, T.; Kang, C. *Biochemistry* **1999**, *38*, 14803.
(10) Lin, I. J.; Gebel, E. B.; Machonkin, T. E.; Westler, W. M.; Markley, J. L. *J. Am. Chem. Soc.* **2003**, *125*, 1464.
(11) Lin, I. J.; Gebel, E. B.; Machonkin, T. E.; Westler, W. M.; Markley, J. L. *Proc. Natl. Acad. Sci. U. S. A.* **2005**, *102*, 14581.
(12) Rose, K.; Shadle, S. E.; Eidsness, M. K.; Kurtz, D. M.; Scott, R. A.; Hedman, B.; Hodgson, K. O.; Solomon, E. I. *J. Am. Chem. Soc.* **1998**, *120*, 10743.
(13) Sun, N.; Dey, A.; Xiao, Z. G.; Wedd, A. G.; Hodgson, K. O.; Hedman, B.; Solomon, E. I. *J. Am. Chem. Soc.* **2010**, *132*, 12639.
(14) Beyer, M. K.; Clausen-Schaumann, H. *Chem. Rev.* **2005**, *105*, 2921.
(15) Grandbois, M.; Beyer, M.; Rief, M.; Clausen-Schaumann, H.; Gaub, H. E. *Science* **1999**, *283*, 1727.
(16) Garcia-Manyes, S.; Liang, J.; Szoszkiewicz, R.; Kuo, T. L.; Fernandez, J. M. *Nat. Chem.* **2009**, *1*, 236.
(17) Evans, E. *Annu. Rev. Biophys. Biomol. Struct.* **2001**, *30*, 105.
(18) Kienberger, F.; Ebner, A.; Gruber, H. J.; Hinterdorfer, P. *Acc. Chem. Res.* **2006**, *39*, 29.
(19) Zheng, P.; Li, H. *J. Am. Chem. Soc.* **2011**, *133*, 6791.
(20) Zheng, P.; Cao, Y.; Li, H. *Langmuir* **2011**, *10*, 5713.
(21) Dietz, H.; Berkemeier, F.; Bertz, M.; Rief, M. *Proc. Natl. Acad. Sci. U. S. A.* **2006**, *103*, 12724.
(22) Dietz, H.; Bertz, M.; Schlierf, M.; Berkemeier, F.; Bornschlogl, T.; Junker, J. P.; Rief, M. *Nat. Protoc.* **2006**, *1*, 80.
(23) Blake, P. R.; Park, J. B.; Bryant, F. O.; Aono, S.; Magnuson, J. K.; Eccleston, E.; Howard, J. B.; Summers, M. F.; Adams, M. W. *Biochemistry* **1991**, *30*, 10885.
(24) Fernandez, J. M.; Li, H. *Science* **2004**, *303*, 1674.
(25) Carrion-Vazquez, M.; Oberhauser, A. F.; Fisher, T. E.; Marszalek, P. E.; Li, H.; Fernandez, J. M. *Prog. Biophys. Mol. Biol.* **2000**, *74*, 63.
(26) Sharma, D.; Perisic, O.; Peng, Q.; Cao, Y.; Lam, C.; Lu, H.; Li, H. *Proc. Natl. Acad. Sci. U. S. A.* **2007**, *104*, 9278.
(27) Oberhauser, A. F.; Marszalek, P. E.; Erickson, H. P.; Fernandez, J. M. *Nature* **1998**, *393*, 181.
(28) Rief, M.; Fernandez, J. M.; Gaub, H. E. *Phys. Rev. Lett.* **1998**, *81*, 4764.
(29) Day, M. W.; Hsu, B. T.; Joshua-Tor, L.; Park, J. B.; Zhou, Z. H.; Adams, M. W.; Rees, D. C. *Protein Sci.* **1992**, *1*, 1494.
(30) Bau, R.; Rees, D. C.; Kurtz, D. M. Jr.; Scott, R. A.; Huang, H.; Adams, M. W. W.; Eidsness, M. K. *J. Biol. Inorg. Chem.* **1998**, *3*, 484.
(31) Kurihara, K.; Tanaka, I.; Chatake, T.; Adams, M. W.; Jenney, F. E. Jr.; Moiseeva, N.; Bau, R.; Niimura, N. *Proc. Natl. Acad. Sci. U. S. A.* **2004**, *101*, 11215.
(32) Depending on the techniques used, different number of residues have been identified to form N−H···S$^{\gamma}$ hydrogen bonds.
(33) Yanagisawa, S.; Banfield, M. J.; Dennison, C. *Biochemistry* **2006**, *45*, 8812.
(34) Marshall, N. M.; Garner, D. K.; Wilson, T. D.; Gao, Y.-G.; Robinson, H.; Nilges, M. J.; Lu, Y. *Nature* **2009**, *462*, 113.
(35) Li, H.; Carrion-Vazquez, M.; Oberhauser, A. F.; Marszalek, P. E.; Fernandez, J. M. *Nat. Struct. Biol.* **2000**, *7*, 1117.

(36) Eaton, W. A.; Lovenberg, W. *Iron-Sulfur Proteins*; Academic Press: New York/London, 1973.
(37) Atherton, N. M.; Garbett, K.; Gillard, R. D.; Mason, R.; Mayhew, S. J.; Peel, J. L.; Stangroom, J. E. *Nature* **1966**, *212*, 590.
(38) Christensen, H. E.; Hammerstad-Pedersen, J. M.; Holm, A.; Iversen, G.; Jensen, M. H.; Ulstrup, J. *Eur. J. Biochem.* **1994**, *224*, 97.
(39) Cao, Y.; Lam, C.; Wang, M. J.; Li, H. B. *Angew. Chem., Int. Ed.* **2006**, *45*, 642.
(40) Cao, Y.; Li, H. *Nat. Mater.* **2007**, *6*, 109.
(41) Carrion-Vazquez, M.; Oberhauser, A. F.; Fowler, S. B.; Marszalek, P. E.; Broedel, S. E.; Clarke, J.; Fernandez, J. M. *Proc. Natl. Acad. Sci. U. S. A.* **1999**, *96*, 3694.
(42) Marko, J. F.; Siggia, E. D. *Macromolecules* **1995**, *28*, 8759.
(43) In order to rupture the FeS_4 center and obtain a ΔL_c of 13 nm, at least two ferric-thiolate bonds from the same CXXC chelating motif need to be ruptured. Thus, the measured rupture force could also include contributions from unfolding of the CXXC chelating loop. However, unfolding of the CXXC loop will result in a length increment of ~1nm, which cannot be resolved by our AFM due to the compliant polypeptide chain.
(44) It is important to note that in addition to the effect of eliminating a backbone hydrogen bond or affecting the strength of the backbone hydrogen bond by the proline or glycine substitutions, it is possible that introduction of a proline or glycine also affects the flexibility of the CXXC chelating loop (proline substitution makes the loop stiffer while glycine substitution makes the loops more flexible) and thus the force needed to unfold the CXXC chelating loop. It is possible that these collective effects contribute to the observed change of the mechanical stability of ferric-thiolate bonds. Nonetheless, these possibilities point to the fact that protein environment plays important roles in modulating the mechanical stability of ferric-thiolate bonds in rubredoxin.
(45) In the same vein, it is equally important to investigate the influence of N−H···S^{γ} hydrogen bonds on the mechanical stability of ferrous-thiolate bond in rubredoxin. Previously, we used the reducing agent dithiothreitol (DTT) to measure the mechanical stability of ferrous-thiolate bond in rubredoxin. However, DTT or other reducing agents are competing ligands for ferrous/ferric ion. Thus, the measured mechanical stability of ferrous-thiolate bonds is potentially complicated by the effect of such competing ligands. Therefore, such experiments call for anaerobic environment in which AFM will be housed or an electrochemical AFM setup. Future endeavors will be required for carrying out such experiments.
(46) Lane, R. W.; Ibers, J. A.; Frankel, R. B.; Holm, R. H. *Proc. Natl. Acad. Sci. U. S. A.* **1975**, *72*, 2868.
(47) Park, I. Y.; Eidsness, M. K.; Lin, I. J.; Gebel, E. B.; Youn, B.; Harley, J. L.; Machonkin, T. E.; Frederick, R. O.; Markley, J. L.; Smith, E. T.; Ichiye, T.; Kang, C. *Proteins* **2004**, *57*, 618.